Performance and Figure of Merit Comparisons for a Macromolecular Diffractometer Located on SNS Beamlines Viewing Different Moderators

J.P. Hodges and C. Rehm
7/15/2004

To compare alternate designs for a macromolecular diffractometer it is useful to evaluate a Figure of Merit, M, for each design or the relative change in M for a particular design choice. In the case of neutron protein crystal diffraction experiments, given the high demand and cost of beam time, the Figure of Merit should be inversely proportional to experiment duration, D_{expt}, for a given protein crystal of volume, V_s. In the regime where all background is intrinsic to the protein crystal Eqn. A.1 is the simplest relationship that possesses the required properties.

$$MV_s D_{\text{expt}} = 1 \qquad \text{Eqn A.1.}$$

For the collection of a complete data set, which encompasses a hemisphere of reciprocal space out to resolution shell d_{min} of interest (typically $d_{\text{min}} = 2$ Å), the beamtime required is

$$D_{\text{expt}} = St \qquad \text{Eqn A.2.}$$

where S is the number of different crystal orientation settings and t is the measurement time for a single crystal setting.

The number of crystal orientation settings, S, can be estimated from the usable detector coverage as it sweeps across the outermost reciprocal resolution shell with optimum instrument wavelength band, λ_{min} to λ_{max}. The usable detector coverage is the volume of reciprocal space where neighboring Bragg reflections are separated and is determined by the instrument resolution function and protein crystal unit-cell symmetry and dimensions. For the analysis presented here, protein crystals will be assumed to be of primitive symmetry (no systematic absences) and cubic of unit-cell dimension, a, and volume, v_{uc}.

The measurement time for a single crystal setting, t, is dictated by the rate limiting component of the measurement. This, in the case of Laue single crystal time-of-flight technique at a pulsed spallation neutron source, is the measurement of Bragg reflections belonging to the outermost resolution shell with sufficient statistical precision. The Bragg reflections belonging to inner resolution shells have, on average, greater intensity and therefore for a given measurement time will be determined to a higher precision than the outer resolution shell reflections. Thus, the measurement time for a single crystal setting can be estimated by combining expressions for signal and background at the outer resolution shell together to form a statistical expression for counting precision.

Here we present an analysis that combines analytical expressions for signal and background with instrument resolution functions determined by detailed Monte Carlo simulations. For SNS beamlines viewing different moderators the figure-of-merit and experiment beamtime functions for cubic protein crystal structures of interest are determined and compared.

Intensity of Bragg Peaks

A single protein crystal diffraction measurement surveys many thousands of individual Bragg peaks with inherently a wide distribution of structure factors and intensities. The intensity of an individual Bragg peak of structure factor, F_{hkl}, is given by

$$I_{hkl} = t\varphi\varepsilon\kappa N_s \frac{\lambda^4}{2v_{uc}\sin^2\theta} \mathrm{T}_{DW} \left|F_{hkl}\right|^2 \qquad \text{Eqn A.3}$$

where I_{hkl} = integrated intensity for peak *hkl* (n),
t = duration of measurement (s),
$\varphi(\lambda)$ = incident neutron flux at sample (n.cm^{-2}.s^{-1}.Å^{-1}),
$\varepsilon(\lambda)$ = detector efficiency,
κ = conversion factor 1×10^{24} (cm^2.bn^{-1}),
N_s = no. of unit cells in sample,
2θ = Bragg angle for reflection,
v_{uc} = unit cell volume (Å^3),
$\mathrm{T_{DW}}$ = temperature factor,
$|F_{hkl}|^2$ = structure factor modulus of reflection *hkl* squared (bn),

For the purpose of determining required measurement time for a single crystal setting, we can average over the nonsystematic variation of structure factors and use the following expression for average Bragg peak intensity

$$I_{\mathrm{pk}} = t\varphi\varepsilon\kappa N_s \frac{\lambda^4}{2v_{uc}\sin^2\theta} \mathrm{T}_{DW} \left\langle \left| F_{hkl} \right|^2 \right\rangle \qquad \text{Eqn A.4}$$

$$= t\varphi\varepsilon\kappa N_s \frac{\lambda^4}{2v_{uc}\sin^2\theta} \mathrm{T}_{DW} n_{\mathrm{ord}} \left\langle b_j^2 \right\rangle \qquad \text{Eqn A.5}$$

$$= t\varphi\varepsilon\kappa N_s \lambda^4 \left[\frac{\mathrm{T}_{DW}}{2\sin^2\theta} \right] \tau_{\mathrm{ord}} \qquad \text{Eqn A.6}$$

where I_{pk} = integrated intensity for an average Bragg peak (n),
n_{ord} = number of ordered atoms in a single protein crystal unit-cell,
$\langle b_j^2 \rangle$ = average coherent scattering length^2 of atoms in ordered crystal structure (bn),
τ_{ord} = $n_{\mathrm{ord}} \left\langle b_j^2 \right\rangle / v_{uc}$
= average ordered crystal structure scattering strength density (bn.Å^{-3}).

Equation A.6 is of note; it is the common form we use for expressing all signal and background components. For a non-deuterated protein crystal with 35% of the solvent water molecules crystallographically ordered, $\tau_{\mathrm{ord}} = 0.0223$ bn.Å^{-3} and similarly, for a fully deuterated protein crystal with D_2O solvent, $\tau_{\mathrm{ord}} = 0.0358$ bn.Å^{-3}.

Background

Since, non-deuterated protein crystals require ~20 times more beam time than deuterated crystals it is rational to optimize MaNDi (and indeed all other protein neutron diffractometers) for deuterated crystals. The cost of protein deuteration by exchange or special synthesis is insignificant when compared to the real cost of extended beam time required. This then necessitates a more detailed model of the intrinsic sample background, rather than assuming that all the background is simply due to the total incoherent scattering cross-section of the protein crystal; as has previously been common practice.

Central to estimating the various background components (the sum of which is the background) it is instructive to first consider the reciprocal volume over which the background is integrated. Defining a reciprocal volume element, v_q^*, as the reciprocal volume per reflection,

$$v_q^* = \frac{1}{v_{uc}} \qquad \text{Eqn A.7}$$

then the reciprocal volume, v^*, integrated over for the determination of both peak, I_{pk}, and background intensity, B_{pk}, can be normalized to a dimensionless quantity, n_{v^*},

$$n_{v^*} = \frac{v^*}{v_q^*} \qquad \text{Eqn A.8}$$

This normalized reciprocal volume, n_{v^*}, is simply the fraction of reciprocal volume per reflection that is used for integration (peak intensity and background under the peak). The underlying integration volume, v^*, is determined by

$$v^* = v_{shell}^* \frac{\Omega_{pk}}{4\pi} 2\sin^2\theta \qquad \text{Eqn A.9}$$

$$v_{shell}^* = \frac{4\pi}{3}\left(\lambda_{min}^{-3} - \lambda_{max}^{-3}\right) = 4\pi\frac{\Delta\lambda}{\lambda^4} \qquad \text{Eqn A.10}$$

where Ω_{pk} = transverse solid angle coverage of Bragg peak on detector (sr).

The use of a normalized reciprocal volume quantity, n_{v^*}, allows simple expressions of the same form to be used for both the peak intensity and background components. In this analysis the three intrinsic background components estimated originate from thermal diffuse scattering, solvent disorder and incoherent scattering.

Modeling the loss of Bragg peak intensity from thermal motion and static partial disorder (as embodied in the temperature factor T_{DW} in Eqn A.4) as an incoherent distribution then the resulting background contribution over a single reciprocal volume element, v_q^*, is given by

$$B_{\text{ord, diff}} = t\varphi\varepsilon\kappa N_s \lambda^4 \left\langle \frac{\left(1 - T_{DW}\right)}{2\sin^2\theta} \right\rangle_{\text{shell}} \tau_{\text{ord}} \qquad \text{Eqn A.11}$$

or $$B_{\text{ord, diff}} = t\varphi\varepsilon\kappa N_s \lambda^4 T'_{\text{diff}} \tau_{\text{ord}} \qquad \text{Eqn A.12}$$

where $$T'_{\text{diff}} = \left\langle \frac{T'_{DW}}{2\sin^2\theta} \right\rangle_{\text{shell}} = \left\langle \frac{2d^2 T'_{DW}}{\lambda^2} \right\rangle_{\text{shell}} \qquad \text{Eqn A.13}$$

Eqn A.12 is of the common form, see Eqn A.6. The factor T'_{diff} is evaluated by averaging the temperature factor complement, $T'_{DW} = 1\text{-}T_{DW}$ over all reflections present in Ewald's sphere of constant λ, in accordance with Eqn A.13. Figure A.1 shows a numerical estimation of the factor T'_{diff} as a function of wavelength for isotropic displacement parameter $B_{\text{iso}} = 20$ Å^2.

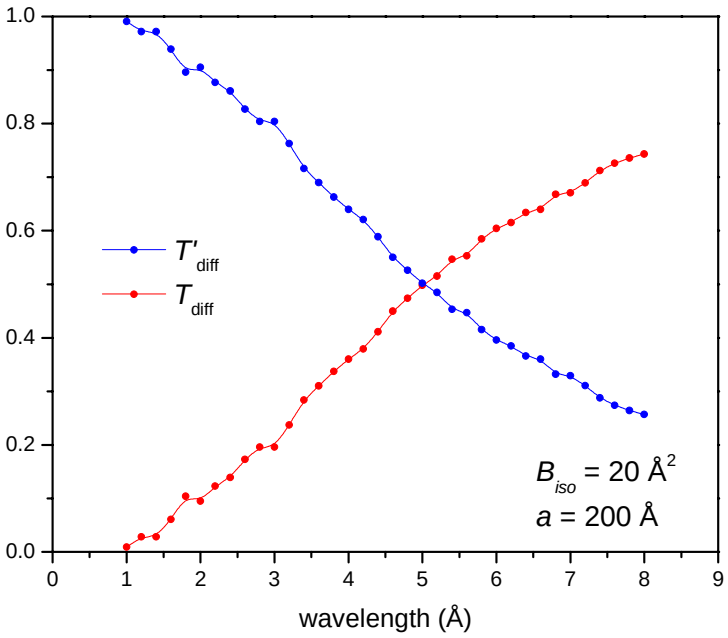

Figure A.1. Numerical average determination of $T'_{\text{diff}} = 1 - T_{\text{diff}}$. (Functions are independent of a over range of interest, a large a value was used to improve statistics)

The background contribution per reciprocal volume element arising from the total coherent cross-section of the disordered solvent molecules present in the protein crystal is given by

$$B_{\mathrm{dis,diff}} = t\varphi\varepsilon\kappa N_s \lambda^4 \tau_{\mathrm{dis}} \qquad \text{Eqn A.14}$$

where τ_{dis} = average disordered crystal structure scattering strength density (bn.Å^{-3}). For a non-deuterated protein crystal with 65% of the solvent water molecules crystallographically disordered, τ_{dis} = 0.0064 bn.Å^{-3} and similarly, for a fully deuterated protein crystal with D_2O solvent, τ_{dis} = 0.0127 bn.Å^{-3}.

The background contribution per reciprocal volume element due to the total incoherent cross-section of all the atoms present in the protein crystal is simply given by

$$B_{\mathrm{inc}} = t\varphi\varepsilon\kappa N_s \lambda^4 \tau_{\mathrm{inc}} \qquad \text{Eqn A.15}$$

where τ_{inc} = incoherent scattering strength density (bn.Å^{-3}). For non-deuterated and fully deuterated protein crystals, τ_{inc} = 0.414 and 0.0107 bn.Å^{-3}, respectively.

By summation the background per reciprocal volume element is

$$B = tF_{\mathrm{eff}} N_s \left[T'_{\mathrm{diff}} \, \tau_{\mathrm{ord}} + \tau_{\mathrm{dis}} + \tau_{\mathrm{inc}} \right] \qquad \text{Eqn A.16}$$

where $F_{\mathrm{eff}} = \varphi\varepsilon\kappa\lambda^4$ (n.Å^3.bn^{-1}.s^{-1}).

Decisive in estimating Bragg peak precision and consequently counting time required for a single orientation, t, is the background intensity located beneath a Bragg peak, B_{pk}. This is simply given by multiply the background per volume element by the normalized reciprocal volume;

$$\begin{aligned} B_{\mathrm{pk}} &= Bn_{v^*} \\ &= tF_{\mathrm{eff}} N_s \left[T'_{\mathrm{diff}} \, \tau_{\mathrm{ord}} + \tau_{\mathrm{dis}} + \tau_{\mathrm{inc}} \right] n_{v^*} \end{aligned} \qquad \text{Eqn A.17}$$

For completeness, the complementary expression for Bragg peak intensity is

$$I_{\mathrm{pk}} = tF_{\mathrm{eff}} N_s \left[\frac{\mathrm{T}_{DW}}{2 \sin^2 \theta} \right] \tau_{\mathrm{ord}} \qquad \text{Eqn A.18}$$

Example A.1:
Peak and background intensities for fully deuterated and non-deuterated protein crystal.
Decoupled H_2-moderator BL-11; incident flux $\varphi = 1.3\times10^7$ n.cm^{-2}.s^{-1}.Å^{-1}and divergence $\Omega_{inc} = 0.56°\times0.56°$.
Pixelated detector module; $2\theta = 90°$, $\varepsilon = 1.0$.
Crystal; $a = 150$ Å, $v_{uc} = 3375000$ Å^3, $V_s = 0.125$ mm^3.
Resolution shell; $d_{min} = 2.0$ Å.
Temperature factors; $B_{iso} = 20$ Å^2, $T_{DW} = 0.08$, $T'_{Diff} = 0.805$.
Normalized reciprocal volume of peaks determined by MC simulation, $n_{v*} = 0.283$.
Single crystal orientation measurement time, $t = 5.5$ days.

	deuterated (n)	**non-deuterated (n)**
$\boldsymbol{I_{pk}}$	**43**	**27**
$B_{ord,diff}$	424	265
$B_{dis,diff}$	187	92
B_{inc}	159	6067
$\boldsymbol{B_{pk}}$	**217**	**1818**

Example A.1 demonstrates that for a fully deuterated (protein + solvent) crystal the background from thermal, solvent disorder and incoherent scattering is ~5 times greater than would be estimated using only the incoherent scattering density. Example A.1 also shows the great difference in signal-to-background ratio between deuterated and non-deuterated protein crystals.

Precision and Single Orientation Measurement Time

Setting an average integrated Bragg peak intensity precision criterion of $P_I = 2.0$ ($P_I = I_{pk}/\sigma_{pk}$) for the Bragg peaks belonging to the outermost resolution shell, the time required for a single orientation crystal diffraction measurement can be estimated using the following statistic for peak above background;

$$\sigma_I = \sqrt{I + \mu B}\,, \qquad \text{Eqn. A.19.}$$

$$\mu = 1 + \frac{n}{2^D(1-n)}\,, \qquad \text{Eqn. A.20.}$$

where μ represents the degradation of the precision caused by background,
D = appropriate dimensionality (= 3 for volume integration),
n = normalized peak width, area, or volume for D = 1, 2, or 3, respectively.

Equation A.20 would be appropriate if standard crystallographic integration software were to use all available volume around a reflection for background determination, however, this is not generally the case and so it is more realistic and conservative to include the proviso $\mu \geq 2$. This has been used in the analysis presented here.

Example A.2. The estimated measurement times for a single crystal orientation for fully deuterated and non-deuterated protein crystals.

Decoupled H_2-moderator BL-11; incident divergence Ω_{inc} = 0.56°×0.56°.
Pixelated detector module; 2θ = 30-170°, ε = 1.0.
Crystal; a = 150 Å, v_{uc} = 3375000 Å^3, V_s = 0.125 mm^3.
Resolution shell; d_{min} = 2.0 Å.
Temperature factors; B_{iso} = 20 Å^2, T_{DW} = 0.08, T'_{Diff} = 0.95 - 0.66.
Normalized reciprocal volume of peaks determined by MC simulation.

2θ (°)	***t* deuterated (days)**	***t* non-deuterated (days)**
45	38.0	720.0
60	10.0	187.0
75	4.9	91.3
90	3.6	57.1
120	3.1	43.3
150	2.0	32.9

The figure-of-merit approach allows the distribution in implied measurement times across a detector array to be combined to yield a single total figure-of-merit for the instrument and from this an appropriately weighted average single measurement time can be calculated. The original figure-of-merit expression A.1 can be partitioned into contributions arising from bands of detector coverage as follows

$$M = \frac{1}{V_S} \sum_{\text{bands}} \frac{w_{\text{band}}}{t_{\text{band}}} \qquad \text{Eqn A.21}$$

where t_{band} = measurement time estimated at center of detector coverage band (days)
w_{band} = appropriate weighting scheme.

Each detector band covers a range of Bragg scattering angle, 2θ, from a minimum angle $2\theta_{\text{band,min}}$ to maximum angle $2\theta_{\text{band,max}}$. The bands, which are of onion ring shape, are adjoining and together represent the entire usable detector area of the instrument.

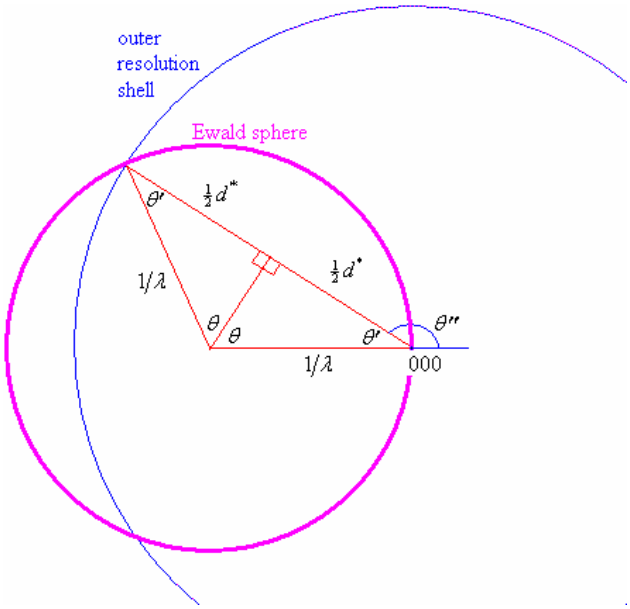

Figure A.2. The Ewald reflecting sphere construction and outer resolution shell.

It is appropriate to weight the contribution of each detector band, w_{band}, by the number of outermost resolution shell Bragg peaks each band will survey during a single crystal orientation measurement or, more simply and equivalent, the hemisphere surface area fraction, f_{hs}, of the outermost resolution shell swept through by each detector band. From the Ewald reflecting sphere construction, shown in Figure A.2,

$$\theta' = \tfrac{\pi}{2} - \theta \qquad \text{Eqn A.22}$$

$$\theta'' = \pi - \theta' = \tfrac{\pi}{2} + \theta \qquad \text{Eqn A.23}$$

the surface area of the outer resolution shell, Ω_{ORS}, swept through by a detector band is

$$\Omega_{\text{ORS}} = 2\pi \int_{\theta''_{\text{band,min}}}^{\theta''_{\text{band,max}}} \sin\theta'' d\theta'' \qquad \text{Eqn A.24}$$

$$= 2\pi \int_{\theta_{\text{band,min}}}^{\theta_{\text{band,max}}} \sin\left(\tfrac{\pi}{2} + \theta\right) d\theta \qquad \text{Eqn A.25}$$

$$= 2\pi \int_{\theta_{\text{band,min}}}^{\theta_{\text{band,max}}} \cos\theta d\theta \qquad \text{Eqn A.26}$$

$$= 2\pi \left[\sin\theta_{\text{band,max}} - \sin\theta_{\text{band,min}}\right] \qquad \text{Eqn A.27}$$

and hence,

$$f_{\text{band,hs}} = \frac{\Omega_{\text{ORS}}}{2\pi} = \left[\sin\theta_{\text{band,max}} - \sin\theta_{\text{band,min}}\right] \qquad \text{Eqn A.28}$$

Eqn A.24 is simply the expression for surface area integration,

$$\Omega = \int \sin\theta d\theta d\phi \qquad \text{Eqn A.29}$$

integrated over all ϕ,

$$\Omega = 2\pi \int \sin\theta d\theta \qquad \text{Eqn A.30}$$

and stated for an individual detector band.

Therefore the expression for figure-of-merit becomes

$$M = \frac{1}{V_S} \sum_{\text{bands}} \frac{f_{\text{hs, band}}}{t_{\text{band}}} \qquad \text{Eqn A.31}$$

As defined earlier, the collection of a complete data set encompasses a hemisphere of reciprocal space out to resolution shell d_{min} of interest, leads directly to quantifying the number of different crystal orientations required, S, through the total reciprocal volume hemisphere fraction, f_{hs}, surveyed by the entire usable detector area;

$$f_{hs} = \sum_{\text{bands}} f_{\text{hs, band}} \qquad \text{Eqn A.32}$$

$$= \left[\sin\theta_{\text{max}} - \sin\theta_{\text{min}}\right] \qquad \text{Eqn A.33}$$

and $$S = f_{\text{hs}}^{-1} . \qquad \text{Eqn A.34}$$

In using all available detector coverage, where Bragg peaks are separate and collecting intensity data out at least to the outer resolution shell, a certain minimum bandwidth is presumed

$$\Delta\lambda_{\text{req}} = 2d_{\text{min}}\left[\sin\theta_{\text{max}} - \sin\theta_{\text{min}}\right] \qquad \text{Eqn A.35}$$

For our purpose, of comparing and evaluating the performance of several different configurations of a 'world class' neutron TOF Laue protein crystal diffractometer, a large detector array can be assumed, therefore with $2\theta_{\text{max}} = 165^{\text{o}}$ the above expression for minimum bandwidth required becomes

$$\Delta\lambda_{\text{req}} = 2d_{\text{min}}\left[1 - \sin\theta_{\text{min}}\right]. \qquad \text{Eqn A.36}$$

The combination of fixed repetition frequency of a spallation neutron source user facility, which for the SNS target station-I is 60 Hz, and fixed total flight path for a diffractometer results in a fixed usable bandwidth, $\Delta\lambda_{\text{BW}}$ uninterrupted by frame overlap. If the bandwidth required (in accordance with equation A.36) is greater than that available, $\Delta\lambda_{\text{req}} > \Delta\lambda_{\text{BW}}$, then additional time for the collection of the full intensity data set is necessary. The amount of additional time required is given by the ratio, ω, according to

$$\omega = \frac{\Delta\lambda_{\text{req}}}{\Delta\lambda_{\text{BW}}} \qquad \text{if } \Delta\lambda_{\text{req}} > \Delta\lambda_{\text{BW}}$$

$$\text{or} \qquad \omega = 1 \qquad \text{if } \Delta\lambda_{\text{req}} \le \Delta\lambda_{\text{BW}} \qquad \text{Eqn A.37}$$

Special care has to be taken in applying a ω ratio > 1, for comparison of different instruments/configurations, since an improved instrument performance may be achievable by using the available bandwidth, $\Delta\lambda_{BW}$, and reducing the ultimate detector coverage, i.e. increase θ_{min} such that $\Delta\lambda_{req} = \Delta\lambda_{BW}$.

Often, the bandwidth required is less than the instrument bandwidth available, $\Delta\lambda_{req} < \Delta\lambda_{BW}$, however, this does not lead to a reduction in measurement time and therefore increased instrument performance and likewise figure-of-merit (our measure of instrument performance) since this implies a change in repetition rate of the spallation neutron source.

Purely in the interest of making performance comparisons across widely different protein unit-cell volumes clearer, a unit cell volume scale factor, $(a/100\text{Å})^3$, is included in the following final expression for figure-of-merit;

$$M = \omega\left(\frac{a}{100}\right)^3 \frac{1}{V_S} \sum_{\text{bands}} \frac{f_{\text{hs, band}}}{t_{\text{band}}} \qquad \text{Eqn A.38}$$

Estimated Performance and Comparison for MaNDi on SNS Beam Lines Viewing Different Moderators

The ultimate design, performance and scientific range of the MaNDi diffractometer will be intimately tied to choice of SNS moderator type by way of beamline. The figure-of-merit analysis and performance estimates presented here are purposely done to determine which is the optimum moderator for a MaNDi instrument and also yield a baseline estimate of performance (experiment measurement times) and scientific range (protein unit-cell and bulk volume). The different moderator types and respective beamlines compared here are stated in Table A.1. Also given in Table A.1 are the comparable beamlines presently available.

Table A.1. SNS moderator types and respective beamlines.

	SNS Beamline Source (used for MC simulations)			
	11	**5**	**8**	**17**
medium	cryogenic-H_2	cryogenic-H_2	room temp.-H_2O	room temp.-H_2O
poison (depth)	cadmium (27 mm)	none	cadmium (15 mm)	cadmium (25 mm)
coupling to reflector	decoupled	coupled	decoupled	decoupled
short name	dec-H_2	cou-H_2	HR-H_2O	HI-H_2O
comparable unassigned beamline	11B	14A	8 or 9	16

HR for high-resolution & HI for high-intensity

Table A.2. Protein crystal and beamline layout parameters used in the MC simulations.

	values					
protein crystal						
mosaicity (FWHM, °)	0.2					
strain (FWHM, %)	0.1					
B_{iso} (Å^2)	20.0					
diameter (mm)	1.0					
moderator (beamline)	dec-H_2 (11)		cou-H_2 (5)		HR-H_2O (8) HI-H_2O (17)	
beamline layout	high resolution	medium intensity	high resolution	medium intensity	high resolution	medium intensity
moderator-guide distance (m)	6.0	6.0	6.0	6.0	6.0	6.0
curved guide section (m)	12.0	12.0	12.0	12.0	0.0	0.0
straight guide section (m)	3.0	4.5	54.0†	55.5†	15.0	16.5
guide-sample distance (m)	3.0	1.5	3.0	1.5	3.0	1.5
sample-detector distance (m)	0.5	0.5	0.5	0.5	0.5	0.5
moderator-sample distance (m)	24.0	24.0	75.0	75.0	24.0	24.0

curved and straight guide sections are of 15 × 15 mm^2 cross-section except † where straight guide section is of ballistic type (first and final 10 m are tapered, central ballistic section is of 25 × 25 mm^2 cross-section).

Monte Carlo simulations for a MaNDi instrument located on the four available beamlines were performed using the IDEAS program. A summary of the protein crystal and beamline layout parameters for each of the instrument configurations simulated is given in Table A.2. Principally, the Monte Carlo resolution simulations for each possible instrument configuration map the usable detector coverage (2θ range) as a function unit-cell parameter, a, and outer resolution shell parameter, d_{min}. Such a map is shown in Figure A.3 for the medium intensity guide system setting (see Table A.2) for protein crystals ranging in unit-cell parameter a = 75 – 200 Å and an outer resolution shell requirement for resolving Bragg peaks of d_{min} = 2 Å.

The medium intensity guide setting configuration is appropriate for a wide range of protein unit-cell volumes and is used here to compare the performance of a MaNDi instrument on each of the available beamlines. With the supermirror guide configuration set to medium intensity mode the incident neutron divergence is Ω_{inc} = 0.565° × 0.565° for $\lambda \geq$ 2.0 Å and the respective neutron fluxes calculated for each beamline are shown in Figure A.4. A typical set of outer resolution shell Bragg peaks (d_{min} = 2 Å) revealing the spatial transverse resolution is shown for detector 2θ = 60° module and beamline-5 MaNDi simulation in Figure A.5. The spatial widths of the Bragg peaks, all ~ 7 mm, are very close to that estimated from convoluting the neutron incident divergence (FW = 0.565°) with the crystal mosaicity (FW ~ 0.6°) and applying a sample-detector distance of 0.5 m; which yields an expected transverse peak width of 7.2 mm. Using the approach described in the previous section, figure-of-merit values for fully deuterated protein crystals were determined for unit-cell size range, a = 100 – 150 Å; these are plotted in Figure A.5 and stated also in Table A.3. From inspection of Figure A.5 it is immediately apparent that the performance of a MaNDi instrument is greatly affected by the choice of beamline/moderator. Comparison between the figure-of-merit functions and their respective beamline fluxes (see Figure A.4) shows that flux on sample is not the dominant factor driving the performance of a macromolecular diffractometer.

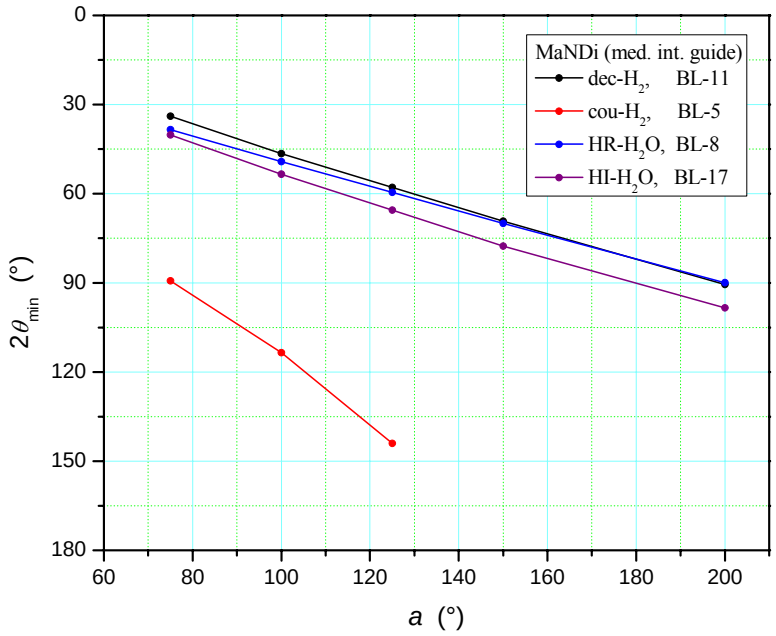

Figure A.3. Minimum usable detector angle, $2\theta_{min}$, for resolvable Bragg peaks determined for MaNDi located on the comparison set of SNS beamlines. The Monte Carlo simulations were performed for outer resolution shell d_{min} = 2 Å.

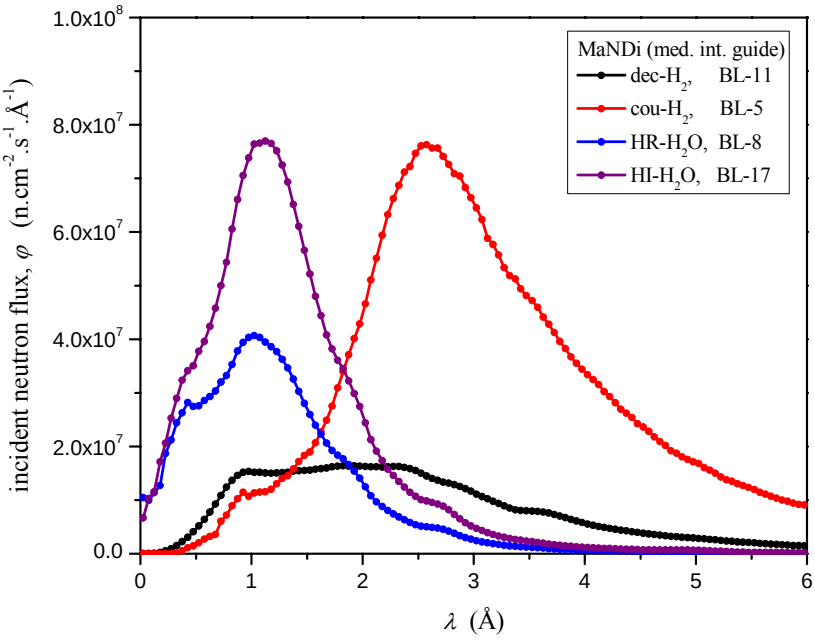

Figure A.4. Neutron fluxes at sample for the comparison set of SNS beamlines with medium intensity guide configuration.

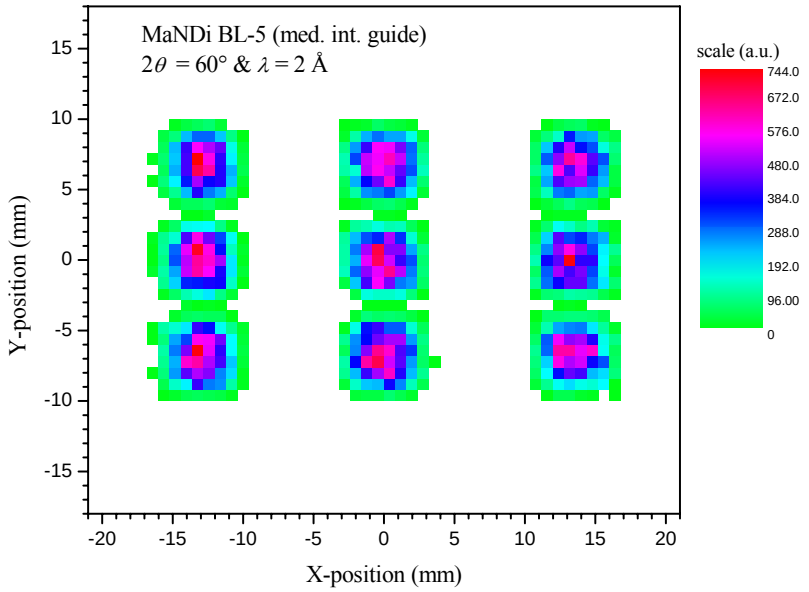

Figure A.5. Simulated Bragg peaks at the detector plane calculated for SNS beamline-5 (cou-H_2 moderator) for protein crystal parameters given in Example A.2. The first green contour is at 2% of peak maximum.

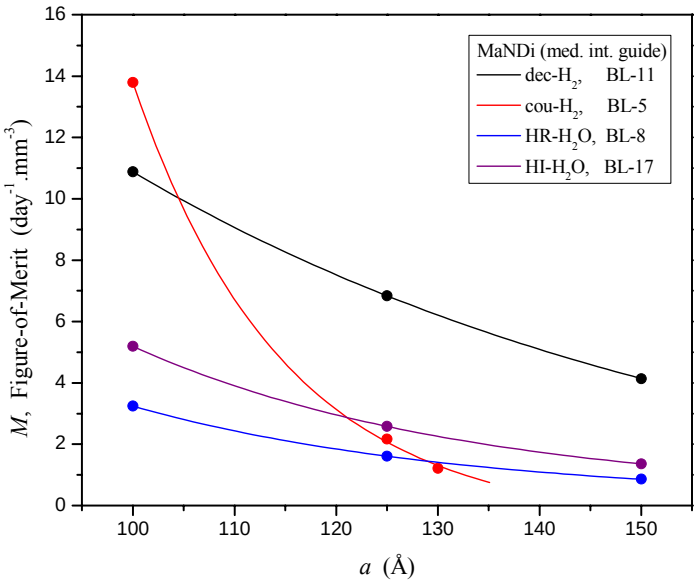

Figure A.6. Figure-of-merit functions determined for fully deuterated protein crystals, d_{min} = 2 Å and MaNDi located on the comparison set of SNS beam lines with medium intensity guide configuration.

Table A.3. Figure-of-merit values and derived measurement time parameters S, t and D_{expt} for fully deuterated protein crystal of volume 0.125 mm^3 and MaNDi located on the comparison set of SNS beam lines with medium intensity guide configuration.

		MaNDi (moderator + beam line)			
		dec-H_2 BL-11	**cou-H_2 BL-5**	**HR-H_2O BL-8**	**HI-H_2O BL-17**
a = 100 Å	M	10.88	13.79	3.24	5.19
	S	1.64	6.44	1.64	1.82
	t	0.45	0.09	1.51	0.85
	D_{expt}	**0.74**	**0.58**	**2.47**	**1.54**
a = 125 Å	M	6.84	2.17	1.61	2.58
	S	1.96	24.00	2.03	2.20
	t	1.17	0.30	4.78	2.75
	D_{expt}	**2.29**	**7.19**	**9.70**	**6.05**
a = 130 Å	M	*6.20*	1.21	*1.41*	*2.25*
	S	2.05	39.20	2.09	2.31
	t	*1.39*	0.37	*5.98*	*3.39*
	D_{expt}	***2.84***	**14.50**	***12.50***	***7.82***
a = 150 Å	M	4.14	-	0.86	1.36
	S	2.39	-	2.39	2.61
	t	2.73	-	13.10	7.60
	D_{expt}	**6.52**	**-**	**31.30**	**19.80**

values in italics are derived by interpolation, see Figure A.6.

With consideration to the biological community's desire to reduce the required size of protein crystals for neutron diffraction, by setting V_s = 0.125 mm^3 the time per crystal orientation and overall data collection time can be derived from the above determined figure-of-merit values (the number of crystal orientation settings, S, is independent of sample volume). The respective values are given in Table A.3.

The calculated performance of each MaNDi instrument is best represented and assessed by a plot of estimated experiment duration versus protein unit-cell parameter; this is shown in Figure A.7. Clearly, the performance of a MaNDi instrument located on the decoupled cryogenic-H_2 moderator beamline-11 is superior to all the other candidate beamlines shown. The difference in performance between the beamline choices is revealed by charting each detector band contribution, M_{band}, to the overall Figure-of-merit, as shown in Figure A.8 for a = 100 Å.

Selecting a coupled cryogenic-H_2 beamline-5 for MaNDi would lead to the quickest measurement times for a single crystal orientation; this is signified by the highest $M_{band}/\Delta 2\theta$ line in Figure A.8. However, this choice of moderator imposes reduced usable detector coverage (see Figure A.3) and consequently, the sum under the $M_{band}/\Delta 2\theta$ curve, which is the figure-of-merit, is not as high as might otherwise be expected. Practically speaking, this corresponds to very high numbers of crystal orientations (relative to MaNDi on the other beamlines) that need to be measured to complete a full hemisphere of diffraction data, see Table A.3. The high number of different orientation measurements required ultimately led to very long measurement times for protein crystals with large unit-cell volumes; see for $a \geq 120$ Å on Figure A.6.

For the two ambient-H_2O moderator beamlines 8 and 17, the difference between their respective MaNDi performances is determined almost exclusively by the much higher neutron flux of beamline-17. However, the peak in effective flux occurs around $\lambda = 1.55$ Å and this is unfavorable to absolute instrument performance in two ways. First, the effective flux peak at $\lambda = 1.55$ Å leads to a peak in the $M_{band}/\Delta 2\theta$ function at $2\theta \sim 50°$ and due to the instrument resolution boundary condition (see Figure A.3) only one side of this function contributes to the overall figure-of-merit, see Figure A.8. Second, independent of neutron flux, the M_{band} values at the forward scattering angles, $2\theta \sim 50°$, are relatively low because of the high peak integration volumes (n_{v*} approaches unity at $2\theta_{min}$) and, consequently, much higher background integrated under the Bragg peaks (compared to respective situation at $2\theta \sim 90°$ appropriate for the cryogenic-H_2 moderators).

Fundamentally, the superior performance of MaNDi located on the decoupled cryogenic-H_2 moderator beamline-11 is because this combination avoids the serious detrimental factors discussed above for the other beamline choices. With a peak in effective flux at $\lambda \sim 3.1$ Å for beamline-11, the $M_{band}/\Delta 2\theta$ function is peaked close to the center of usable detector coverage, and consequently both sides of this peaked function contribute to the overall figure-of-merit. The large usable detector coverage results in the lowest number of different crystal orientation measurements required to complete a full hemisphere of data collection. Significantly, and differing from all the other candidate beamlines, the lower resolution boundary, $2\theta_{min}$, for MaNDi on beamline-11 occurs away from the peak in the $M_{band}/\Delta 2\theta$ function, resulting in the lowest rise (gradient) in estimated experiment durations versus protein unit-cell parameter.

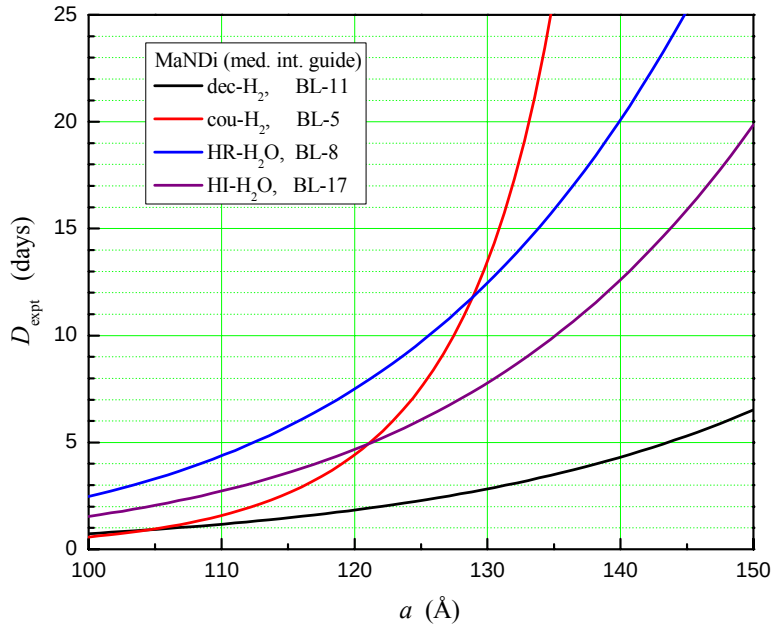

Figure A.7. Estimated experiment durations as a function of protein unit-cell parameter for a fully deuterated protein crystal of volume 0.125 mm^3, d_{min} = 2 Å and MaNDi located on the comparison set of SNS beam lines with medium intensity guide configuration.

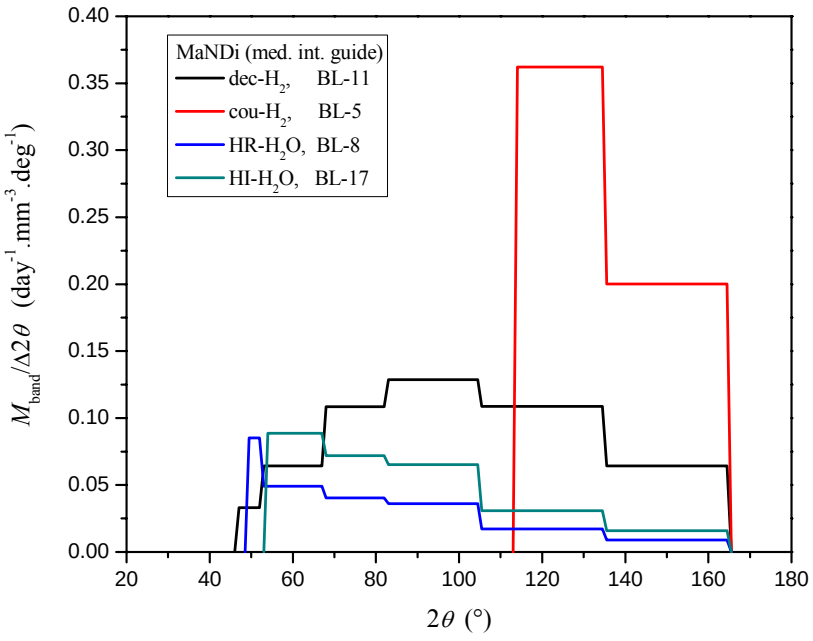

Figure A.8. Figure-of-merit contributions from the individual detector bands.